

Article

Evolution of the Shadow Effect with Film Thickness and Substrate Conductivity on a Hemispherical Workpiece during Magnetron Sputtering

Huaiyuan Liu ¹, Donglin Ma ^{2,*}, Yantao Li ¹, Lina You ¹ and Yongxiang Leng ^{1,3,*}

¹ Key Laboratory of Advanced Technologies of Materials, Ministry of Education, School of Materials Science and Engineering, Southwest Jiaotong University, Chengdu 610031, China

² College of Physics and Engineering, Chengdu Normal University, Chengdu 611130, China

³ Sichuan Province International Science and Technology Cooperation Base of Functional Materials, College of Medicine, Southwest Jiaotong University, Chengdu 610031, China

* Correspondence: mdl208115@163.com (D.M.); yxleng@swjtu.edu.cn (Y.L.); Tel.: +86-28-87601149 (Y.L.); Fax: +86-28-87601149 (Y.L.)

Highlights:

What are the main findings?

1. There is a threshold thickness and incident angle below which the film is unaffected by the shadow effect during DC magnetron sputtering.
2. The later-deposited film causes the earlier-deposited film to be affected by the shadow effect.
3. The shadow effect manifests earlier for films deposited on the insulator SiO₂ than for those deposited on the semiconductor Si.

What is the implication of the main finding?

1. There is no need to worry about the shadow effect when the film deposited by oblique incident deposition has small thickness or the incident angle is small.
2. The conductivity of the substrate could influence the shadow effect.



Citation: Liu, H.; Ma, D.; Li, Y.; You, L.; Leng, Y. Evolution of the Shadow Effect with Film Thickness and Substrate Conductivity on a Hemispherical Workpiece during Magnetron Sputtering. *Metals* **2023**, *13*, 165. <https://doi.org/10.3390/met13010165>

Academic Editor: Cătălin-Daniel Constantinescu

Received: 28 November 2022

Revised: 7 January 2023

Accepted: 11 January 2023

Published: 13 January 2023



Copyright: © 2023 by the authors. Licensee MDPI, Basel, Switzerland. This article is an open access article distributed under the terms and conditions of the Creative Commons Attribution (CC BY) license (<https://creativecommons.org/licenses/by/4.0/>).

Abstract: When depositing films on a complex workpiece surface by magnetron sputtering, the shadow effect occurs and causes the columnar structure to tilt toward the substrate owing to the oblique incident angle of the plasma flux, affecting the microstructure and properties of the films. Improving the surface diffusion could alleviate the shadow effect, whereas changing the energy of the deposited particles could improve surface diffusion. Different substrate conductivities could affect the energy of the deposited particles when they reach the substrate. In this study, Si (semiconductor) and SiO₂ (insulator) sheets are mounted on the inner surface of a hemispherical workpiece, and Ti films with different thicknesses (adjusted by the deposition time) are deposited on the inner surface of the hemispherical workpiece by direct current magnetron sputtering. The results show that there is a threshold thickness and incident angle before the films are affected by the shadow effect. The threshold could be affected by the film thickness, the incident angle, and the conductivity of the substrate. The threshold would decrease as the film thickness or incidence angle increased or the conductivity of the substrate decreased. When the film thickness or incident angle does not reach the threshold, the film would not be affected by the shadow effect. In addition, the film deposited later would tilt the vertical columnar structure of the film deposited earlier. Owing to the different conductivities, the shadow effect manifest earlier for Ti films deposited on the insulator SiO₂ than for films deposited on the semiconductor Si when the film thickness is >500 nm.

Keywords: magnetron sputtering; oblique incident deposition; shadow effect; film thickness; substrate conductivity

1. Introduction

Magnetron sputtering is a plasma-based surface modification technology with a high deposition rate, low substrate temperature, and high film–substrate adhesion [1]. It is an important method for improving the performance and service life of the workpiece [2]. However, when depositing films on a complex workpiece surface, oblique incident deposition is inevitable. Oblique incident deposition implies the substrate surface and deposition source (such as a sputtering target) deposited at a certain angle. The shadows would be cast across the substrate because of the oblique plasma flux with the growth of the random distribution nuclei. The shadow effect [3] would appear and affect the growth of the film. Because of the shadow effect, the growth of the columnar crystal in the shadow would be suppressed. The faster-growing columnar crystals would inhibit the slower-growing columnar crystals and result in the columnar structure of the film tilted to the substrate. The shadow effect would be stronger when the incidence angle becomes larger. The shadow effect can generate pores in the film [4], which may decrease the hardness of the film [5]. However, the shadow effect can also decrease the density of the film [6], which could influence the corrosion resistance of the films.

According to previous studies, the scattering of deposited particles before reaching the substrate contributes to the shadow effect, and the scattering is affected by changing the distance from the target to the substrate or the working pressure. When the distance between the target and substrate is significant, the shadow effect would be strong [7], whereas a higher working pressure can suppress the shadow effect [8–10]. Under low working pressures, the ballistic deposition regime dominates and atoms tend to form an inclined columnar structure, whereas, under high working pressures, the diffusive regime dominates and atoms tend to form a vertical columnar structure [10]. Hawkeye et al. [11] determined that surface diffusion can compete with the shadow effect. The deposited particles would diffuse from the initial nucleation point to the shadow area due to their own surface diffusion during the oblique incidence deposition, suppressing the preferred growth of columnar structure caused by the shadow effect. However, surface diffusion needs to surmount a certain energy barrier [12], when the shadow effect becomes stronger, the energy barrier to overcome would be higher [13], so the diffusion would be suppressed. The high ionization degree of high-power pulsed magnetron sputtering can improve surface diffusion so that it can efficiently suppress the shadow effect [14–16]. However, the energy of the deposited particles can affect surface diffusion [17]. The energy of the deposited particles could be affected by the electric field provided by the bias. The substrate conductivity would affect the strength of the electric field provided by the bias. Under the same bias, the substrate conductivity affects the energy of the deposited particles when they reach the substrate, influencing the surface diffusion and shadow effect. Therefore, the energy of particles could be increased by changing the conductivity of the substrate, which could improve the surface diffusion and then suppress the shadow effect.

Notably, the crystal orientation of the film influences surface diffusion [17,18]. It implies that different orientations of the crystal of the film could promote or suppress surface diffusion. For the same deposition process, different film thicknesses would affect the crystal orientation [19,20]. That implies the film thickness could suppress the shadow effect by influencing the crystal orientation to promote surface diffusion.

In this study, Si (which is a semiconductor) and SiO₂ (which is an insulator) with different conductivity were mounted on the inner surface of a hemispherical workpiece, and Ti films with different thicknesses (adjusted by the deposition time) were deposited on this inner surface by direct current (DC) magnetron sputtering. The evolution of the shadow effect with the film thickness and substrate conductivity was studied. The influence of the shadow effect on the structure of the Ti films was investigated and discussed.

2. Materials and Methods

Ti films were deposited on the inner surface of a hemispherical workpiece (diameter 100 mm), and the workpiece was installed on a substrate holder with a target-to-substrate

distance of 60 mm. A rectangular Ti target ($135 \times 170 \text{ mm}^2$) was placed inside the vacuum chamber. The Si (100) and SiO_2 samples ($20 \times 10 \text{ mm}^2$) were mounted on the inner surface of the hemispherical workpiece (Figure 1). The incident angles of the sample at 90° , 60° , 30° , and 0° corresponded to positions at 90° , 60° , 30° , and 0° from the center of the hemispherical workpiece to the perpendicular line of the target. The incident angles and the target-to-substrate distance of the sample at different positions in the hemispherical workpiece were different. The sample with a large incidence angle would have a small target-to-substrate distance, while the sample with a small incidence angle would have a large target-to-substrate distance.

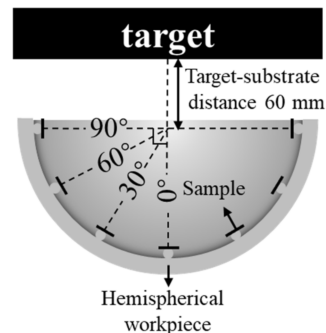


Figure 1. Schematic of the target, hemispherical workpiece, and sample position.

After the vacuum chamber was pumped to a base pressure of $2.0 \times 10^{-3} \text{ Pa}$, the target was cleaned by DC magnetron sputtering (DCMS, 2 A) for 10 min, and the substrate was cleaned by glow discharge with Ar ions (3.6 Pa; applied DC bias voltage, -1500 V) for 25 min. The Ti film was then deposited by DCMS (3 A) with a DC substrate bias (-150 V) at 0.65 Pa and the film thicknesses were approximately 300, 500, and 1000 nm. The film thickness would decrease with the increase of incident angle and increase with the decrease of the target-to-substrate distance. This indicated that the thickness of the deposited film might not change significantly.

X-ray diffractometer (XRD, Empyrean-XRD, Netherlands) was used to determine the crystal structure of the films prepared. The anode target of the X-ray diffractometer was a Cu target ($\lambda = 1.54060 \text{ \AA}$). The X-ray tube voltage was 40 kV, and the current was 40 mA. The selected scanning range of Ti film was $30^\circ \sim 45^\circ$. Scanning Electron Microscope (SEM, JSM-7800F, JEOL, Japan) was used to observe the cross-sectional morphology of the Ti films. The electronic acceleration voltage was 5 kV, the working distance was 10 mm, and the magnification was 60 thousand times. The software called ImageJ was used to semiquantitative analyze the porosity of different films by calculating gray value, and the porosity of different films was $<0.1\%$.

3. Results and Discussion

In this work, in order to investigate the influence of the crystal orientation and the energy of the deposited particles on the surface diffusion and shadow effect, the crystal orientation of the surface would be adjusted by changing the film thickness, and the energy of the deposited particles would be adjusted by selecting semiconductor and insulator as substrate. The evolution of the shadow effect with the film thickness and substrate conductivity would be studied.

3.1. Cross-Sectional Morphology

The cross-sectional morphologies of the Ti films deposited on the Si substrate at incident angles of 90° , 60° , 30° , and 0° with film thicknesses of 300, 500, and 1000 nm are shown in Figure 2. When the thickness of the Ti film was approximately 300 nm (Figure 2a), the columnar structures of the samples deposited at different incident angles were perpendicular to the substrate without the influence of the shadow effect. When the thickness of the Ti film was approximately 500 nm (Figure 2b), the columnar structures

of the samples deposited at incident angles of 0° and 30° were perpendicular to the substrate, without the influence of the shadow effect. The columnar structures of the samples deposited at incident angles of 60° and 90° had oblique angles of approximately 20° and 38° with the normal line of the substrate, respectively, under the influence of the shadow effect. When the thickness of the Ti film was approximately 1000 nm (Figure 2c), the columnar structures of the samples deposited at incident angles of 30° , 60° , and 90° had oblique angles of approximately 14° , 22° , and 46° , respectively, with the normal line of the substrate, under the influence of the shadow effect.

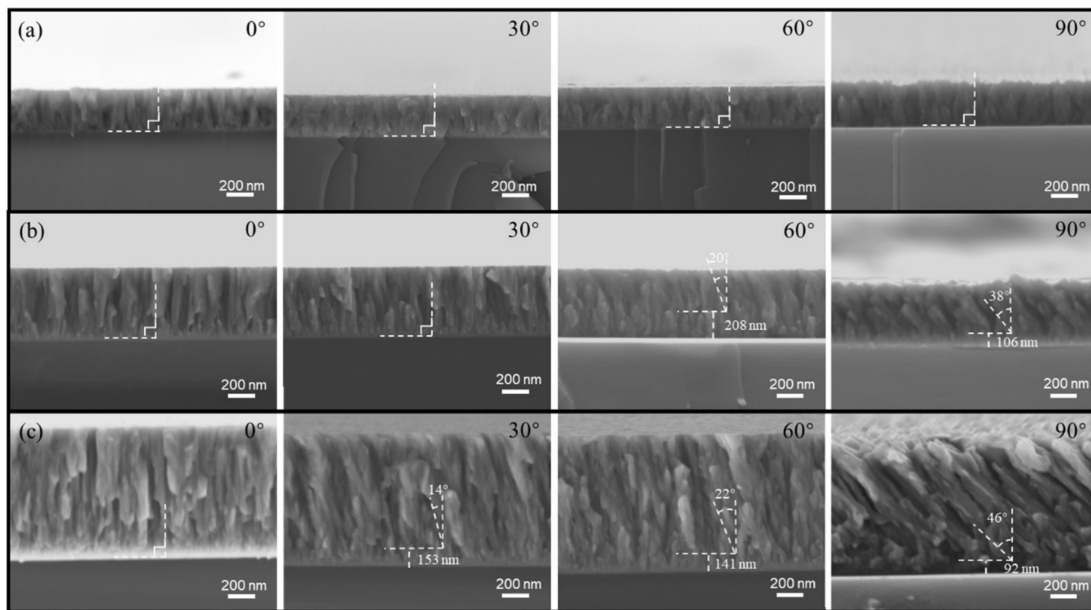


Figure 2. Cross-sectional morphology of Ti films deposited on Si substrates with film thicknesses of 300 nm (a), 500 nm (b), and 1000 nm (c).

These results indicate that the threshold of the incident angle, under the influence of the shadow effect, decreases as the thickness of the Ti film increases. These values are listed in Table 1. When the film thickness was approximately 300 nm, the samples deposited at different incident angles were unaffected by the shadow effect. When the film thicknesses were approximately 500 and 1000 nm, the thresholds of the incident angles affected by the shadow effect were 60° and 30° , respectively. As the film thickness increased, the threshold of the incident angles decreased, and the film was more easily affected by the shadow effect.

Table 1. Incident angle thresholds affected by the shadow effect on the Si substrate.

Sample	Si		
	300 nm	500 nm	1000 nm
Threshold of incident angle ($^\circ$)	-	60	30

Further analysis of the samples affected by the shadow effect indicated that with increasing film thickness, the columnar structure of the film exhibited an unexpected response. The film deposited later caused the film deposited earlier to be affected by the shadow effect. In particular, when the film thickness was approximately 300 nm, the samples deposited at an incident angle of 60° were not affected by the shadow effect, indicating that the thickness threshold of the sample affected by the shadow effect was >300 nm. However, when the film thicknesses were increased to 500 and 1000 nm, the film thickness thresholds of the sample under the influence of the shadow effect decreased to

208 and 153 nm, respectively. This suggests that as the film thickness increases, the film thickness threshold of the sample affected by the shadow effect decreases.

For the other samples affected by the shadow effect, the film thickness threshold is listed in Table 2. This threshold decreased with an increase in the film thickness and incident angle.

Table 2. Film thickness threshold of samples affected by the shadow effect on the Si substrate.

Sample	Film Total Thickness (nm)	Si			
		0°	30°	60°	90°
Threshold of film thickness (nm)	300	-	-	-	-
	500	-	-	208	106
	1000	-	153	153	92

The cross-sectional morphologies of the Ti films deposited on the SiO₂ substrate at incident angles of 90°, 60°, 30°, and 0° with film thicknesses of 300, 500, and 1000 nm are shown in Figure 3. When the thickness of the Ti film was approximately 300 nm (Figure 3a), the columnar structure of the samples deposited at an incident angle of 90° was affected by the shadow effect and exhibited an oblique angle of approximately 35° with the normal line of the substrate because the substrate was SiO₂ (insulator). In contrast, when the substrate was Si with the same film thickness, the columnar structure of the samples deposited at an incident angle of 90° was perpendicular to the substrate without the shadow effect.

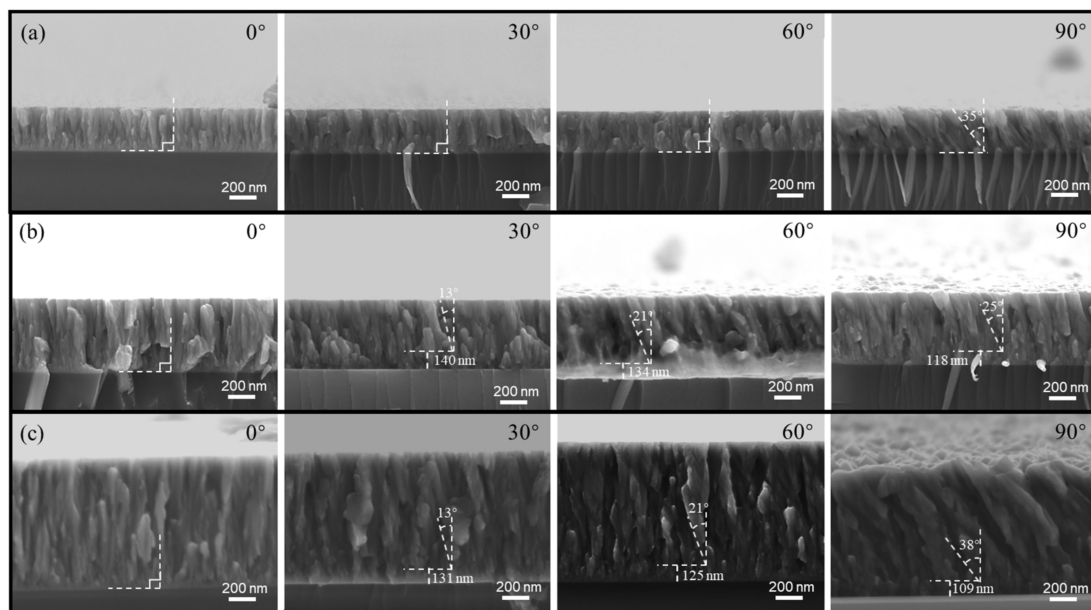


Figure 3. Cross-sectional morphology of Ti films deposited on SiO₂ substrates with film thicknesses of 300 nm (a), 500 nm (b), and 1000 nm (c).

When the substrate was SiO₂ and the thickness of the Ti film was approximately 500 nm (Figure 3b), the columnar structures of the samples deposited at incident angles of 30°, 60°, and 90° were affected by the shadow effect and had oblique angles of approximately 13°, 21°, and 25° with the normal line of the substrate, respectively. In contrast, when the substrate was Si with the same film thickness, the columnar structure of the samples deposited at an incident angle of 30° was perpendicular to the substrate without the shadow effect. The columnar structures of the samples deposited on Si at incident angles of 60° and 90° exhibited oblique angles of approximately 20° and 38° with the normal line of the substrate, respectively, under the influence of the shadow effect.

When the substrate was SiO₂ and the thickness of the Ti film was approximately 1000 nm (Figure 3c), the columnar structures of the samples deposited at incident angles of 30°, 60°, and 90° were affected by the shadow effect and exhibited oblique angles of approximately 13°, 21°, and 38° with the normal line of the substrate, respectively. These results indicate that the threshold of the incident angles affected by the shadow effect decreases as the thickness of the Ti film increases when the Ti film is deposited on SiO₂.

As summarized in Table 3, when the film thicknesses are 300, 500, and 1000 nm, the thresholds of the incident angles affected by the shadow effect are 90°, 30°, and 30°, respectively. As the film thickness increased, the threshold of the incident angle became smaller, and the film was more readily affected by the shadow effect. In particular, when the film thickness was approximately 500 nm, the incident angle threshold of the Ti film on Si affected by the shadow effect was 60°, whereas that of the Ti film on SiO₂ affected by the shadow effect was 30°. This indicates that the lower the conductivity of the substrate, the more readily the prepared Ti film is affected by the shadow effect. The conductivity of the substrates could influence the energy of the deposited particles, and the energy of the deposited particles on a substrate with high conductivity would be higher than that on a substrate with low conductivity under the same bias. Therefore, the difference between the conductivities of the substrates may affect surface diffusion. As the conductivity of SiO₂ was lower than that of Si, the substrate bias provided a lower electric field strength; consequently, the energy of the deposited particles could not be increased, and the Ti film was affected by the shadow effect.

Table 3. Incident angle thresholds affected by the shadow effect on a SiO₂ substrate.

Sample	SiO ₂		
	300 nm	500 nm	1000 nm
Threshold of incident angle (°)	90	30	30

As shown in Figure 3, the Ti films deposited on SiO₂ affected by the shadow effect are similar to those deposited on Si. At the beginning of the deposition of samples affected by the shadow effect, the columnar structure grew perpendicular to the substrate without the shadow effect. The columnar structure of the film appeared inclined to the normal line of the substrate when the thickness of the film exceeded the threshold value. The film thickness thresholds of the samples deposited on SiO₂ under the shadow effect are listed in Table 4. In order to better compare the film thickness thresholds of Ti films on the two substrates, the vertical growth thickness of columnar structures of films on different substrates is shown in Figure 4. The results suggest that these thresholds decrease with increasing film thickness and incident angle. This also indicates that the lower the conductivity of the substrate, the more readily the prepared Ti film is affected by the shadow effect. In addition, it was suggested that the film deposited later would cause the film deposited earlier to be affected by the shadow effect. The reason for this phenomenon has not yet been determined. According to the research [21], the temperature of the substrate would increase, which might influence the structure of the deposited film as the thickness of the film (the deposition time) increases. How temperature would affect the columnar structure of the film would be explored and reported subsequently.

Table 4. Film thickness thresholds of samples affected by the shadow effect on a SiO₂ substrate.

Sample	Film Thickness (nm)	SiO ₂			
		0°	30°	60°	90°
Threshold of film thickness (nm)	300	-	-	-	0
	500	-	140	134	118
	1000	-	131	125	109

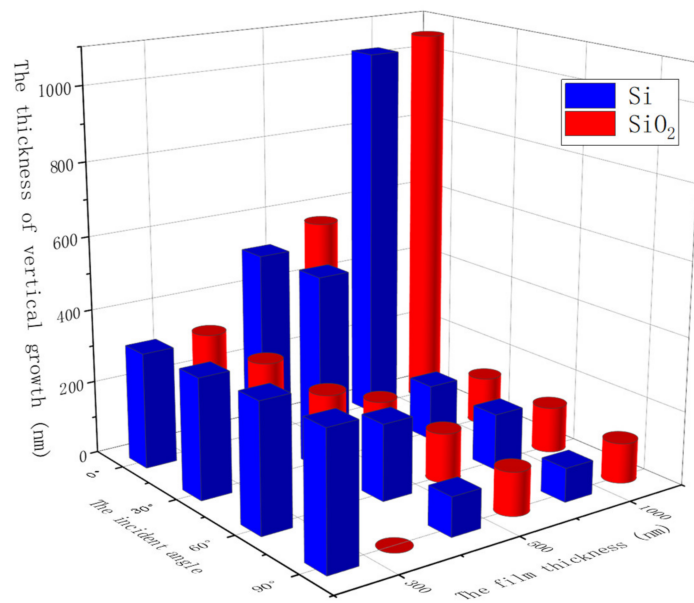


Figure 4. Vertical growth thickness of columnar structures of films on different substrates.

3.2. XRD

The XRD patterns of Ti films deposited on Si and SiO₂ with different film thicknesses at different positions are shown in Figure 5. The Ti films on Si and SiO₂ at 0° exhibited a preferred (100) orientation with different film thicknesses. At an incident angle of 90°, the crystal orientation of the Ti films on Si changed with increasing film thickness. When the film thickness did not exceed the film thickness threshold, the film exhibited a preferred (100) orientation. The film exhibited a (100)-(101) mixed orientation when the film thickness exceeded the film thickness threshold. The Ti films deposited on SiO₂ exhibited a (100)-(002)-(101) mixed orientation when the film thickness was approximately 300 nm. This is because the film thickness threshold was <300 nm. The Ti films revealed a (100) preferred orientation when the film thickness was approximately 500 nm and finally revealed a (100)-(101) mixed orientation when the film thickness was approximately 1000 nm.

The texture coefficient (TC) of the Ti deposited on a different substrate with different deposition times was shown in Figure 6. When the incident angle was 0°, the TC of Ti films on different substrates did not change significantly with time. When the incident angle was 90°, TC (100) decreased, and TC (002) and TC (101) increased as the deposition time increased on Si. As for Ti film deposited on SiO₂, TC (100) increased as the deposition time increased from 3 min to 5 min and decreased as the deposition time increased from 5 min to 10 min. TC (002) and TC (101) decreased as the deposition time increased from 3 min to 5 min and increased as the deposition time increased from 5 min to 10 min.

During deposition, owing to the sample being parallel to the target (0°), the deposited particles continuously bombarded the film vertically, leading to an increase in the strain energy in the film. With an increase in the film thickness, the strain energy in the film increased, leading to an increase in the relative diffraction intensity of the Ti (100) crystal face [22]. At an incident angle of 90°, the crystal faces of the (002) and (101) planes increased when the film was affected by the shadow effect. In addition, with increasing film thickness, the plasma continuously heated the substrate, which led to a gradual increase in the relative diffraction intensity of the Ti (101) crystal face [23]. Thus, the relative diffraction intensity of the (101) crystal plane increased with increasing film thickness. The crystal orientation of the film influences surface diffusion [17,18]. Under the same deposition process, different film thicknesses would affect the crystal orientation [19,20]. Therefore, the change in the orientation of the crystal for the film on SiO₂ at 90° may influence surface diffusion.

The thickness of the vertical growth of the film on SiO₂ at 90° with a film thickness of approximately 300 nm was different from the pattern observed in this study.

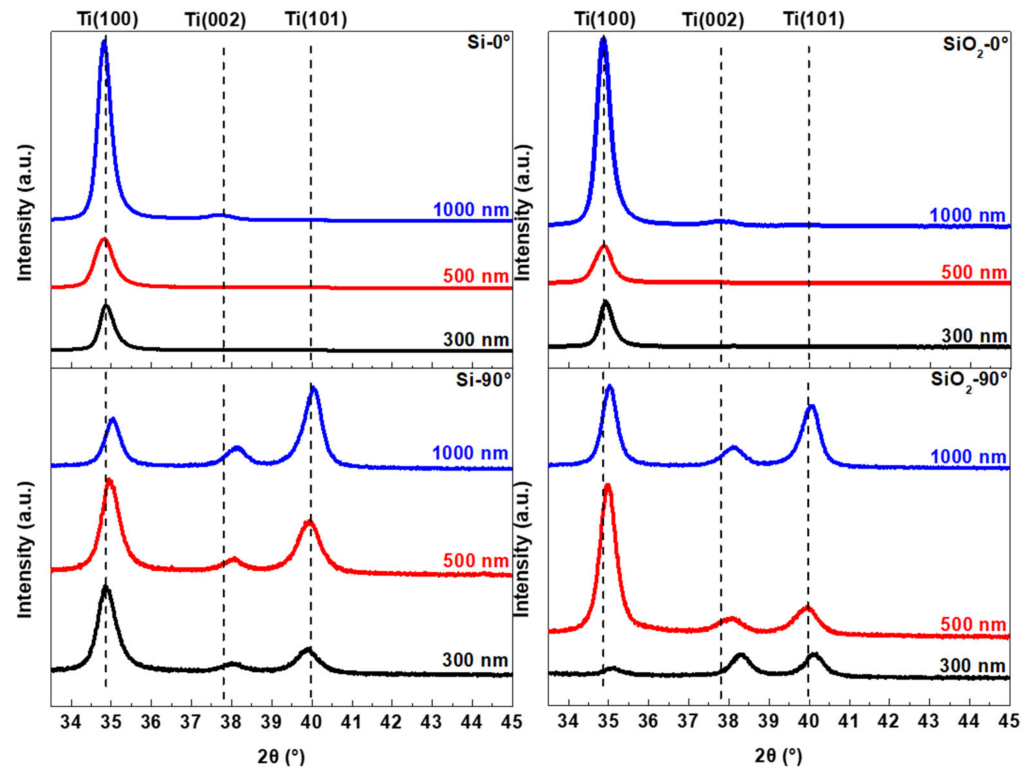


Figure 5. XRD patterns of Ti films deposited on Si and SiO₂ at 0° and 90° with different film thicknesses.

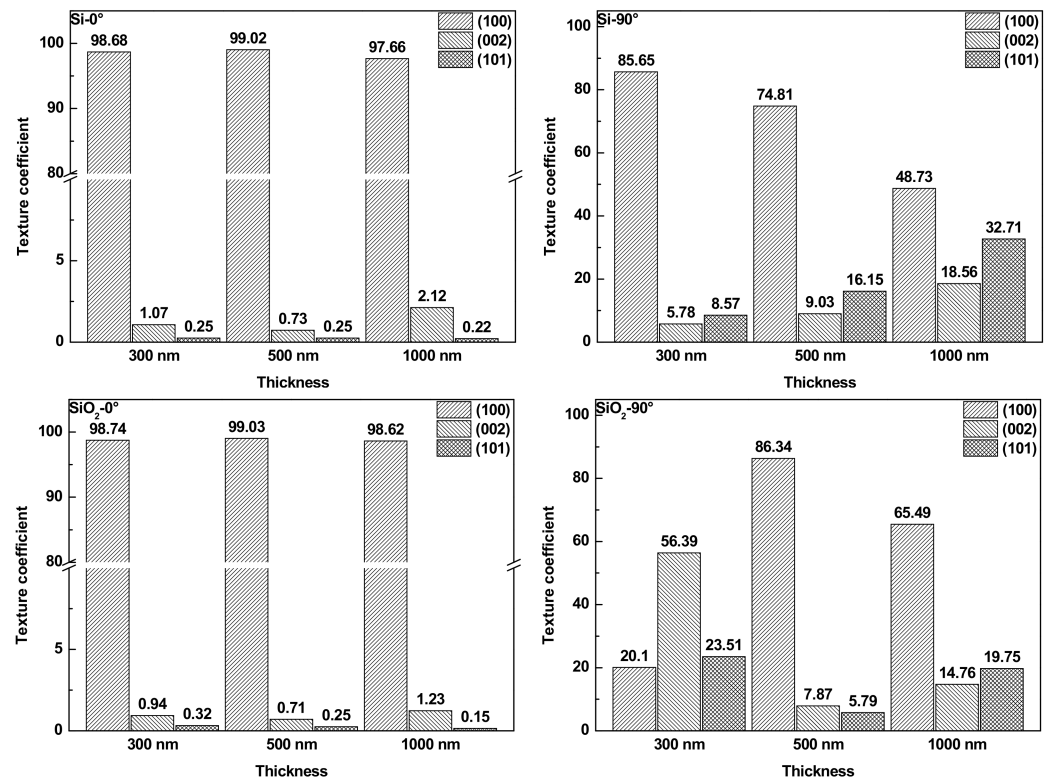


Figure 6. Texture coefficient of the Ti films deposited on Si and SiO₂ at 0° and 90° with different film thicknesses.

In this work, Si (semiconductor) and SiO₂ (insulator) with different conductivity were mounted on the inner surface of a hemispherical workpiece, and Ti films with different thicknesses (adjusted by the deposition time) were deposited on this inner surface by direct current magnetron sputtering (DCMS). The effect of changes in film thickness and substrate conductivity on surface diffusion and shadow effect was investigated and discussed.

4. Conclusions

In this study, two types of substrates (Si and SiO₂) with different conductivities were mounted on the inner surface of a hemispherical workpiece, and Ti films with different thicknesses (adjusted by the deposition time) were deposited on the inner surface by DC magnetron sputtering. The main results are summarized as follows.

The incident angle threshold of the sample affected by shadow effects decreases as the thickness of Ti film increased, and the film thickness threshold of the sample affected by the shadow effect decreases with the increase of the film thickness and the incident angle. When the film thickness or incident angle is below the threshold, the film would not be affected by the shadow effect. As such, the Ti film was deposited on Si, and when the film thickness was <300 nm, the film was not affected by the shadow effect. When the film thickness is below the threshold, the crystal structure of the film would not be affected by the shadow effect. When the Ti film is affected by the shadow effect, the TC (002) and TC (101) would increase while the TC (100) decreases. The film deposited later would tilt the vertical columnar structure of the film deposited earlier, and this would reduce the threshold of the thickness and incident angles of the films before being affected by the shadow effect. Compared with the Ti film deposited on Si substrate, the columnar structure of Ti film deposited on SiO₂ substrate was affected by the shadow effect earlier. This suggests that the substrates with poor electrical conductivity would be more susceptible to the shadow effect.

Author Contributions: Conceptualization, Y.L. (Yongxiang Leng); methodology, Y.L. (Yongxiang Leng); software, Y.L. (Yongxiang Leng); validation, Y.L. (Yongxiang Leng), D.M. and H.L.; formal analysis, H.L.; investigation, H.L.; resources, Y.L. (Yongxiang Leng); data curation, Y.L. (Yongxiang Leng); writing—original draft preparation, H.L.; writing—review and editing, Y.L. (Yongxiang Leng), D.M. and Y.L. (Yantao Li); visualization, H.L. and L.Y.; supervision, Y.L. (Yongxiang Leng); project administration, Y.L. (Yongxiang Leng); funding acquisition, Y.L. (Yongxiang Leng) and D.M. All authors have read and agreed to the published version of the manuscript.

Funding: This research was funded by the Science and Technology on Surface Physics and Chemistry Laboratory (No. 6142A02190402), and Sichuan Science and Technology Program (2020YFH0044, 2021YFH0032).

Data Availability Statement: Data available on request from the authors.

Conflicts of Interest: The authors declare no conflict of interest.

References

1. Musil, J.; Vlček, J. A perspective of magnetron sputtering in surface engineering. *Surf. Coat. Technol.* **1999**, *112*, 162–169. [[CrossRef](#)]
2. Kelly, P.; Arnell, R. Magnetron sputtering: A review of recent developments and applications. *Vacuum* **2000**, *56*, 159–172. [[CrossRef](#)]
3. Verbeno, C.; Krohling, A.; Paschoa, A.; Bueno, T.; Soares, M.; Mori, T.; Larica, C.; Nascimento, V.; van Lierop, J.; Passamani, E.C. Cobalt nanowire arrays grown on vicinal sapphire templates by DC magnetron sputtering. *J. Magn. Mater.* **2020**, *507*, 166854. [[CrossRef](#)]
4. Santos, R.; Chuvilin, A.; Modin, E.; Rodrigues, S.; Carvalho, S.; Vieira, M. Nanoporous thin films obtained by oblique angle deposition of aluminum on porous surfaces. *Surf. Coat. Technol.* **2018**, *347*, 350–357. [[CrossRef](#)]
5. Phae-ngam, W.; Horprathum, M.; Chananonwathorn, C.; Lertvanithphol, T.; Samransuksamer, B.; Songsiriritthigul, P.; Nakajima, H.; Chaiyakun, S. Oblique angle deposition of nanocolumnar TiZrN films via reactive magnetron co-sputtering technique: The influence of the Zr target powers. *Curr. Appl. Phys.* **2019**, *19*, 894–901. [[CrossRef](#)]
6. Feng, C.; Zhang, W.; Wang, J.; Ma, H.; Liu, S.; Yi, K.; He, H.; Shao, J. Broadband antireflection film by glancing angle deposition. *Opt. Mater.* **2021**, *111*, 110720. [[CrossRef](#)]

7. Haque, S.; Rao, K.; Misal, J.; Tokas, R.; Shinde, D.; Ramana, J.; Rai, S.; Sahoo, N. Study of hafnium oxide thin films deposited by RF magnetron sputtering under glancing angle deposition at varying target to substrate distance. *Appl. Surf. Sci.* **2015**, *353*, 459–468. [[CrossRef](#)]
8. Bouaouina, B.; Mastail, C.; Besnard, A.; Mareus, R.; Nita, F.; Michel, A.; Abadias, G. Nanocolumnar TiN thin film growth by oblique angle sputter-deposition: Experiments vs. simulations. *Mater. Des.* **2018**, *160*, 338–349. [[CrossRef](#)]
9. Liu, H.; Deng, Q.; Ma, D.; Li, Y.; Huang, N.; Leng, Y. The uniformity of TiN films deposited on the inner surfaces of a hemispherical workpiece by high-power pulsed magnetron sputtering. *Int. J. Mod. Phys. B* **2019**, *33*, 1950329. [[CrossRef](#)]
10. Garcia-Martin, J.-M.; Alvarez, R.; Romero-Gomez, P.; Cebollada, A.; Palmero, A. Tilt angle control of nanocolumns grown by glancing angle sputtering at variable argon pressures. *Appl. Phys. Lett.* **2010**, *97*, 173103. [[CrossRef](#)]
11. Hawkeye, M.; Brett, M. Glancing angle deposition: Fabrication, properties, and applications of micro- and nanostructured thin films. *J. Vac. Sci. Technol. A Vac. Surf. Film.* **2007**, *25*, 1317–1335. [[CrossRef](#)]
12. Hao, J.; Jin, S.; Lu, G.-H.; Xu, H. Migration energy barriers and diffusion anisotropy of point defects on tungsten surfaces. *Comput. Mater. Sci.* **2020**, *184*, 109893. [[CrossRef](#)]
13. Sbiaai, K.; Boughaleb, Y.; Mazroui, M.; Hajjaji, A.; Kara, A. Energy barriers for diffusion on heterogeneous stepped metal surfaces: Ag/Cu(110). *Thin Solid Film.* **2013**, *548*, 331–335. [[CrossRef](#)]
14. Oliveira, J.; Ferreira, F.; Anders, A.; Cavaleiro, A. Reduced atomic shadowing in HiPIMS: Role of the thermalized metal ions. *Appl. Surf. Sci.* **2018**, *433*, 934–944. [[CrossRef](#)]
15. Jiang, F.; Zhang, T.; Wu, B.; Yu, Y.; Wu, Y.; Zhu, S.; Jing, F.; Huang, N.; Leng, Y. Structure, mechanical and corrosion properties of TiN films deposited on stainless steel substrates with different inclination angles by DCMS and HPPMS. *Surf. Coat. Technol.* **2016**, *292*, 54–62. [[CrossRef](#)]
16. Bobzin, K.; Bagcivan, N.; Immich, P.; Bolz, S.; Alami, J.; Cremer, R. Advantages of nanocomposite coatings deposited by high power pulse magnetron sputtering technology. *J. Mater. Process. Technol.* **2009**, *209*, 165–170. [[CrossRef](#)]
17. Lai, M.-C.; Park, S.; Seol, Y. An energy stable finite difference method for anisotropic surface diffusion on closed curves. *Appl. Math. Lett.* **2022**, *127*, 107848. [[CrossRef](#)]
18. Li, Y.; Bao, W. An energy-stable parametric finite element method for anisotropic surface diffusion. *J. Comput. Phys.* **2021**, *446*, 110658. [[CrossRef](#)]
19. Shiraishi, T.; Katayama, K.; Yokouchi, T.; Shimizu, T.; Oikawa, T.; Sakata, O.; Uchida, H.; Imai, Y.; Kiguchi, T.; Konno, T.; et al. Effect of the film thickness on the crystal structure and ferroelectric properties of (Hf_{0.5}Zr_{0.5})O₂ thin films deposited on various substrates. *Mater. Sci. Semicond. Process.* **2017**, *70*, 239–245. [[CrossRef](#)]
20. Feng, W.; Zhou, H.; Chen, F. Impact of thickness on crystal structure and optical properties for thermally evaporated PbSe thin films. *Vacuum* **2015**, *114*, 82–85. [[CrossRef](#)]
21. Grigoriev, F.; Sulimov, V.; Tikhonravov, A. Atomistic simulation of the glancing angle deposition of SiO₂ thin films. *J. Non-Cryst. Solids* **2019**, *512*, 98–102. [[CrossRef](#)]
22. Chen, A.; Bu, Y.; Tang, Y.; Wang, Y.; Liu, F.; Xie, X.; Gu, J. Deposition-rate dependence of orientation growth and crystallization of Ti thin films prepared by magnetron sputtering. *Thin Solid* **2015**, *574*, 71–77. [[CrossRef](#)]
23. Chawla, V.; Jayaganthan, R.; Chawla, A.; Chandra, R. Morphological study of magnetron sputtered Ti thin films on silicon substrate. *Mater. Chem. Phys.* **2008**, *111*, 414–418. [[CrossRef](#)]

Disclaimer/Publisher’s Note: The statements, opinions and data contained in all publications are solely those of the individual author(s) and contributor(s) and not of MDPI and/or the editor(s). MDPI and/or the editor(s) disclaim responsibility for any injury to people or property resulting from any ideas, methods, instructions or products referred to in the content.